Radiation Physics and Chemistry 225 (2024) 112110

Contents lists available at ScienceDirect

Radiation Physics and Chemistry

journal homepage: www.elsevier.com/locate/radphyschem

Monte Carlo calculation of the photon beam quality correction factor k_{Q,Q_0} for ionization chambers of very small volume: Use of variance reduction techniques driven with an ant colony algorithm

A.M. Garví [a], L.I. Zamora [b], M. Anguiano [a,c], A.M. Lallena [a,c,*], S. García-Pareja [d]

[a] Departamento de Física Atómica, Molecular y Nuclear, Universidad de Granada, E-18071 Granada, Spain
[b] Servicio de Física y Protección Radiológica, Hospital Reg. Univ. Virgen de las Nieves, E-18014 Granada, Spain
[c] Instituto de Investigación Biosanitaria (ibs.GRANADA), Complejo Hospitalario Universitario de Granada/Universidad de Granada, E-18016 Granada, Spain
[d] U. G. C. Radiofísica Hospitalaria, Hospital Universitario Regional de Málaga, Avda. Carlos Haya s/n, E-29010 Málaga, Spain

ARTICLE INFO

Keywords:
Ant colony algorithm
Splitting
Russian roulette
Monte Carlo
PENELOPE
Ionization chamber
Beam quality correction factor

ABSTRACT

Purpose : To evaluate the effectiveness of an ant colony algorithm in implementing variance reduction techniques in the Monte Carlo computation of the photon beam quality correction factor k_{Q,Q_0} for ionization chambers characterized with very small active volumes.

Methods: The Monte Carlo code PENELOPE has been utilized to compute the photon beam quality correction factor k_{Q,Q_0} for the Semiflex 3D 31021 ionization chamber, which has an active volume of 0.071 cm^3. Various clinical photon beams generated with nominal potentials from 4 to 25 MV have been considered, with a ^{60}Co beam serving as the reference. The calculation involved determining the absorbed dose to both water and the sensitive volume of the ionization chamber. This information was used to derive the $f_{c,Q}$ factors for the photon beams and the f_{c,Q_0} factor for the ^{60}Co beam, whose ratio provides the k_{Q,Q_0} factors.

Results: The algorithm has been initially validated by comparing with analog simulations where no variance reduction techniques are applied. The results have demonstrated an efficiency improvement ranging from a factor of 7 to 44. By incorporating the ant colony algorithm along with the variance reduction techniques, the determination of TPR_{10}^{20} values for various studied photon beams has been achieved. The calculated k_{Q,Q_0} factors agree with previously published values. Two distinct protocols outlined in the TRS-398 have been taken into account and the results obtained for these protocols were compared to explore any differences between them.

Conclusions: The ant colony algorithm facilitates the automatic application of variance reduction techniques, such as splitting and Russian roulette, without the need to delve into the geometric intricacies of the simulation. This automated approach results in increased efficiency, enabling simulations to be conducted within reasonable times while maintaining uncertainties at levels that ensure reliability.

1. Introduction

According to Spencer-Attix cavity theory, for a beam quality Q, the dose to water at a given point $\mathbf{r}$, $D_{w,Q}(\mathbf{r})$, and the absorbed dose to an air cavity situated at the same point, $D_{air,Q}(\mathbf{r})$, are related as

$$D_{w,Q}(\mathbf{r}) = D_{air,Q}(\mathbf{r}) \cdot (s_{w,air})_Q \,. \tag{1}$$

Here $(s_{w,air})_Q$ denotes the ratio of the stopping powers of water and air for the quality Q. Dosimetry codes of practice in radiotherapy, such as TG51 (Almond et al., 1999) and TRS-398 (International Atomic Energy Agency, 2000), recommend determining the absorbed dose on the base of standards of dose to water, using an ionization chamber as a dosimeter. Since these detectors differ from the ideal air cavity considered in the Spencer-Attix theory, a new equation relating $D_{w,Q}(\mathbf{r})$ to the dose determined with the ionization chamber situated at the same point $\mathbf{r}$, $D_{c,Q}(\mathbf{r})$, must be used:

$$D_{w,Q}(\mathbf{r}) = D_{c,Q}(\mathbf{r}) \cdot (s_{w,air})_Q \cdot p_{c,Q} \,. \tag{2}$$

In this equation, $p_{c,Q}$ represents an overall perturbation factor that accounts for various effects due to the fact that the materials from

* Corresponding author at: Departamento de Física Atómica, Molecular y Nuclear, Universidad de Granada, E-18071 Granada, Spain.
E-mail addresses: agarviespi@correo.ugr.es (A.M. Garví), lignacio.zamora.sspa@juntadeandalucia.es (L.I. Zamora), mangui@ugr.es (M. Anguiano), lallena@ugr.es (A.M. Lallena), salvador.garcia.sspa@juntadeandalucia.es (S. García-Pareja).

https://doi.org/10.1016/j.radphyschem.2024.112110
Received 19 September 2023; Received in revised form 19 May 2024; Accepted 4 August 2024
Available online 6 August 2024

which the ionization chamber is constructed are not equivalent to water, the medium in which the measurements are conducted.

In practice, the dose to water is related to the measurement of the ionization chamber, $M_{\mathrm{Q}}(\mathbf{r})$, through the equation:

$$D_{\mathrm{w,Q}}(\mathbf{r}) = M_{\mathrm{Q}}(\mathbf{r}) \cdot N_{D,\mathrm{w,Q}}\,, \tag{3}$$

where $N_{D,\mathrm{w,Q}}$ denotes a calibration factor provided by primary or secondary reference laboratories. However, calibrating any ionization chamber for any beam quality Q is impractical and typically a reference ionization chamber is calibrated for a reference beam of quality Q_0 (often a ^{60}Co gamma beam). Eq. (3) is then reformulated as:

$$D_{\mathrm{w,Q}}(\mathbf{r}) = M_{\mathrm{Q}}(\mathbf{r}) \cdot N_{D,\mathrm{w,Q_0}} \cdot k_{\mathrm{Q,Q_0}}\,, \tag{4}$$

where

$$k_{\mathrm{Q,Q_0}} = \frac{N_{D,\mathrm{w,Q}}}{N_{D,\mathrm{w,Q_0}}} \tag{5}$$

is the beam quality correction factor.

Although $k_{\mathrm{Q,Q_0}}$ can be determined experimentally, the challenges associated with the experimental procedure make its determination via Monte Carlo simulations much more feasible, provided that a detailed description of the geometry of the ionization chamber is available, allowing for accurate modeling. In this scenario, it is possible to assess the mean absorbed dose to the active volume of the ionization chamber, $D_{\mathrm{c,Q}}(\mathbf{r})$, and calculate the ratio:

$$f_{\mathrm{c,Q}} = \frac{D_{\mathrm{w,Q}}(\mathbf{r})}{D_{\mathrm{c,Q}}(\mathbf{r})}\,, \tag{6}$$

where $D_{\mathrm{w,Q}}(\mathbf{r})$ is obtained by using a very small water volume located at $\mathbf{r}$ as the scoring voxel. The beam quality correction factor is then computed as:

$$k_{\mathrm{Q,Q_0}} = \frac{f_{\mathrm{c,Q}}}{f_{\mathrm{c,Q_0}}}\,. \tag{7}$$

Here $f_{\mathrm{c,Q_0}}$ is the factor defined in Eq. (6) but for the reference quality Q_0.

Generally, the computation of $D_{\mathrm{c,Q}}(\mathbf{r})$ through Monte Carlo simulations encounter significant uncertainties, primarily because the active volume of the chamber is usually filled with air, a material where the energy deposition due to photons is notably inefficient, with very low statistics. This issue becomes even more pronounced when dealing with small volume ionization chambers. To address this limitation without escalating the number of simulated histories (*i. e.*, maintaining the simulation CPU time), variance reduction techniques (VRTs) have been widely employed.

In this context, when estimating a given quantity, the key parameter is the efficiency, ϵ, of the employed procedure, defined as:

$$\epsilon = \frac{\bar{q}^2}{\sigma^2(\bar{q})}\,\frac{1}{t_{\mathrm{CPU}}}\,. \tag{8}$$

Here $\bar{q}$ is the Monte Carlo estimate of the quantity of interest, $\sigma(\bar{q})$ is its uncertainty and t_{CPU} is the CPU time required to complete the calculation. VRTs are implemented to enhance the efficiency of the calculation, aiming to diminish $\sigma(\bar{q})$ without increasing t_{CPU}. A comprehensive overview of the main characteristics of VRTs considered in Monte Carlo simulations of radiation-matter interaction processes can be found in the work by García-Pareja et al. (2021).

Numerous studies have employed VRTs in Monte Carlo simulations of the response of ionization chambers (both cylindrical and plane-parallel) to clinical photon beams. The majority of these studies utilized the EGSnrc code (Mainegra-Hing et al., 2003; Buckley et al., 2004; Capote et al., 2004; Sánchez-Doblado et al., 2005; Buckley and Rogers, 2006; Ubrich et al., 2008; Wulff et al., 2008a,b; Bouchard et al., 2009; González-Castaño et al., 2009; Muir and Rogers, 2010; Wulff et al., 2010a,b; Malkov and Rogers, 2018; Shanmugasundaram and Chandrasekaran, 2018; Watson et al., 2018; Campos et al., 2019; Pimpinella et al., 2019; Tikkanen et al., 2020; Alissa et al., 2022) or EGS4 (Ma and Nahum, 1995; Grimbergen et al., 1998; Sánchez-Doblado et al., 2003). Additionally, a few works conducted Monte Carlo simulations using PENELOPE (Sempau et al., 2011; Reis and Nicolucci, 2016; Giménez-Alventosa et al., 2020; Tikkanen et al., 2020). EGSnrc calculations (and also the older ones with EGS4) incorporated several VRTs implemented in the user code `egs_chamber`. These VRTs were correlated sampling (Ma and Nahum, 1993; Buckley et al., 2004), photon splitting (Kawrakow and Fippel, 2000), range-based Russian roulette for electrons, photon cross section enhancement and intermediate phase-space storage (Wulff et al., 2008b), and bremsstrahlung splitting, both directional (Kawrakow et al., 2004) and uniform (Watson et al., 2018). Works utilizing PENELOPE made use of particle splitting, Russian roulette, and interaction forcing VRTs (Salvat, 2019; García-Pareja et al., 2021).

Typically, the application of all these VRTs necessitates a prior analysis of the simulation geometry to determine the specific locations where each technique should be activated. In previous works, an ant colony algorithm (ACA) that overcomes this drawback was developed (García-Pareja et al., 2007; García-Pareja, 2012; García-Pareja et al., 2021). This algorithm facilitates the automatic application of multiple VRTs without explicitly considering the intricate details of the simulation geometry.

In the current study, we have adapted this algorithm to calculate beam quality correction factors for ionization chambers utilized in dosimetry. After outlining the specific characteristics of the adapted algorithm and providing details regarding PENELOPE, our chosen Monte Carlo code, we have described the geometrical setups utilized for computing the beam quality correction factors. Additionally, we have presented details about the geometry of the Semiflex 3D 31021 ionization chamber (PTW, 2017), that we have selected for testing the algorithm capabilities due to its small active volume. The Results section includes, first, the validation of the algorithm that has been conducted comparing the doses obtained in simulations including ACA with those found in analog simulations. Using also the algorithm, the quality indices TPR_{10}^{20} have been calculated for the photon beams of Brualla et al. (2019). Subsequently, we have computed the corresponding quality correction factors for the photon beams sourced from Sheikh-Bagheri and Rogers (2002) and Brualla et al. (2019). Finally, the computed $k_{\mathrm{Q,Q_0}}$ have been compared with previous studies where the beam quality correction factors for this ionization chamber were experimentally measured (Delfs et al., 2019) and simulated (Delfs et al., 2019; Tikkanen et al., 2020).

2. Materials and methods

2.1. Variance reduction techniques and ant colony algorithm

In situations where scoring statistics is very limited, the use of VRTs becomes essential to achieve accurate results within reasonable CPU processing times. Specifically, in the case of small ionization chambers, the occurrence of energy depositions within the active volume is notably low. This is attributed to the small size of the chamber and the fact that the material filling it is air.

As previously mentioned, VRTs are strategies designed to decrease the relative uncertainty of a specific quantity of interest within a given simulation time, without altering its expectation value. To achieve this goal, it is necessary to introduce a statistical weight associated with each simulated particle. Typically, primary particles (those emitted from the source) are assigned a weight $w = 1$. Throughout the particle transport, any method that reduces the variance can be applied, as long as w is adjusted to maintain the expected value of the calculated quantity unchanged.

For a given number of showers,[1] N, the Monte Carlo estimator of a quantity q is expressed as follows:

$$\bar{q} = \frac{1}{N}\sum_{i=1}^{N}\left(\sum_{k} w_k\, q_{ik}\right), \tag{9}$$

where q_{ik} represents the kth contribution to q of the ith shower, and w_k is the weight of the particle producing that contribution. The variance of $\bar{q}$ is estimated as:

$$\sigma^2_{\bar{q}} = \sqrt{\frac{1}{N}\left[\frac{1}{N}\sum_{i=1}^{N}\left(\sum_{k} w_k\, q_{ik}\right)^2 - \bar{q}^2\right]}. \tag{10}$$

In Monte Carlo simulations aimed at calculating the deposited energy within a small region of interest (RoI) embedded in a large geometry, such as the scenario investigated in this study, VRTs like *splitting* and *Russian roulette* prove to be highly efficient. These techniques are effective because their fundamental principle is to favor the radiation flux toward the RoI and suppress radiation moving away from it. This strategy conserves computational resources by avoiding the simulation of particle transport that is unlikely to significantly contribute to the scoring.

Splitting involves transforming a particle with a weight w, which is in a certain state, into s copies with a weight $w' = w/s$. This transformation is applied when the particle is perceived to be "approaching" the RoI. Conversely, when a particle appears to be moving away from the RoI, an increase in simulation efficiency is achieved through the application of *Russian roulette*. In this technique, the particle is killed with a probability K and, if it survives, its weight is augmented by a factor $(1-K)^{-1}$.

Regrettably, there are no universal guidelines for the application of these techniques, given their high dependence on the specific characteristics of the problem at hand. A methodology to overcome this drawback, based on an ant colony algorithm (ACA), has demonstrated particular efficacy in Monte Carlo simulations of radiation transport across diverse problems, including clinical electron linacs (García-Pareja et al., 2007, 2010b), photon dosimetry with MOSFETs (Carvajal et al., 2009), radiosurgery photon beams (García-Pareja et al., 2010a), monoisocentric beam split technique (Cenizo et al., 2011) or calculation of specific absorbed fractions (Díaz-Londoño et al., 2015). This is the procedure that has been adapted in the present work for the case of ionization chambers.

The ACA is rooted in the algorithm initially proposed by Dorigo et al. (1996), inspired by the collective behavior of ant colonies in their search for food. In this natural process, ants discovering food sources return to the nest, leaving trails of pheromones. Paths leading to food sources are then followed by more ants, increasing the pheromone levels and guiding others to these sources.

In the implementation employed in this study, the simulation geometry as a whole has been divided into a set of virtual volume cells. Each cell was characterized by a value denoted as *importance*, I, akin to the role of pheromones in the ACA. I serves as the parameter that effectively governs the ACA. Formally, importance is defined as the probability that particles entering a specific virtual cell will contribute to the quantity of interest. Recognizing that this probability may depend on the particle energy, E, and type, p (electron, photon, or positron in this case), the importance is expressed as a function $I = I(x, y, z, E, p)$, where x, y and z are the spatial coordinates corresponding to the virtual cell.

In its basic form, the algorithm operates on the principle of applying splitting to particles as they transition from one virtual cell to another with a higher I value. Conversely, Russian roulette is applied when I decreases. The I values associated with all virtual cells enable the creation of an *importance map*, a dynamic object for the handling of which the simulation is divided into two parts. The map is initialized from the information gathered from the first one, during which the VRTs are not applied. Subsequently, the map is updated during the second part of the simulation run, wherein VRTs are employed as described earlier.

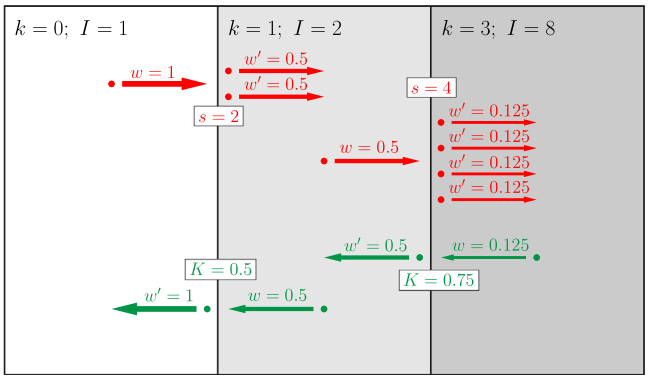

Fig. 1. Scheme illustrating how ACA works in the particle transport.

Let $\mathcal{W}_i^{(\mathrm{T})}$ denote the total weight of particles entering the ith cell; let $\mathcal{W}_i^{(\mathrm{C})}$ be the total weight of particles entering that cell and that are characterized in such a way that either they or any of their descendants subsequently reach the RoI, producing a contribution to the quantity of interest. The fraction

$$P(i) = \frac{\mathcal{W}_i^{(\mathrm{C})}}{\mathcal{W}_i^{(\mathrm{T})}} \tag{11}$$

serves as an estimate of the probability that a particle entering the ith cell will contribute to the quantity of interest.

In principle, importance can be defined as any increasing function with a minimum when $P(i) = 0$ (indicating that none of the particles entering the ith cell reaches the RoI and contributes to the quantity of interest) and a maximum when $P(i) = 1$ (indicating that all particles entering the ith cell reach the RoI and contribute to the quantity of interest). However, it is helpful to impose that all particles arriving at the RoI have a similar weight. This ensures that the variance is prevented from increasing due to uncontrolled weight artifacts.

To achieve this, considering that the minimum value of the splitting factor is 2, the importance function of any virtual cell is defined as a power of 2 as follows:

$$I_i = 2^{[k_i]}, \tag{12}$$

where the subindex refer to the ith cell, $[k_i]$ denotes the closest integer to k_i, and

$$k_i \equiv \begin{cases} 7\,\dfrac{P_i - P_0}{P_0}, & \text{if } P_i \le P_0, \\ 5\,\dfrac{P_i - P_0}{1 - P_0}, & \text{if } P_i > P_0 \end{cases}. \tag{13}$$

In the preceding equation, the quantity P_0 represents the probability that a primary particle, or any of its descendants, arrives at the RoI and contributes to the quantity of interest. The numerical coefficients in the definition of Eq. (13) results in values for the exponent $[k_i]$ ranging from -7 to 5. Practical experience suggests that moderate variations in these coefficients do not lead to significant improvements in the effectiveness of the algorithm.

Once a suitable importance map is obtained in the first part of the simulation, splitting and Russian roulette VRTs are initiated. When a transported particle with weight w moves from the virtual ith cell to the virtual fth cell,

- if $w\, I_f > 1$, the particle is split into $s = w\, I_f$ particles, each one with weight $w' = w/s = I_f^{-1}$;

[1] A shower or history is formed by the trajectories of the primary particle and all the secondary particles it produces.

- if $w\,I_f < 1$, Russian roulette is applied with killing probability $K = 1 - w\,I_f$; when the particle survives, it is assigned the weight $w' = w\,(1-K)^{-1} = I_f^{-1}$, and
- if $w\,I_f = 1$, no action is taken.

This particle transport procedure is schematically illustrated in Fig. 1. Let us assume a particle with $w = 1$ moving from a virtual cell with $I_i = 1$ to another with $I_f = 2$. In this case, splitting occurs with a splitting factor $s = 2$ and in the new cell one has two particles, identical to the previous one, but with a weight $w' = 0.5$. If $I_i = 2$ and $I_f = 8$, the initial particle splits into four identical particles: in the case shown in the figure, the initial particle that has $w = 0.5$ gives rise to four particles with $w' = 0.125$. On the other hand, if a particle moves from a cell with a given importance I_i to another cell with importance $I_f < I_i$, Russian roulette is triggered. For example, if a particle with $w = 0.5$ moves from a $I_i = 2$ cell to a $I_f = 1$ cell, Russian roulette with killing probability $K = 0.5$ is applied and, if the particle survives, it continues moving in the new cell with $w' = 1$. Something similar happens in the other case shown in the figure for a particle moving between the $I_i = 8$ and $I_f = 2$ virtual cells: if this particle survives after applying Russian roulette with $K = 0.75$, its weight increases from $w = 0.125$ to $w' = 0.5$.

It is worth noting that all particles moving in a given cell have a weight equal to the inverse of the importance of this cell, regardless of their previous evolution. This is crucial because ensuring that particles contributing to a specific quantity of interest all have even weights helps to keep the variance of that quantity relatively small (García-Pareja et al., 2021).

The use of this ACA allows VRTs to be applied automatically with minimal user intervention.

2.2. PENELOPE code

In this work we have utilized PENELOPE (Salvat, 2019), a code capable of simulating the transport of electrons, positrons and photons in matter with energies ranging from 100 eV to 1 TeV. Photons are simulated in a detailed manner, considering interaction by interaction. For electrons and positrons, a mixed algorithm is employed, categorizing events as either hard or soft. Hard events involve angular deflections and/or energy losses exceeding certain user-defined threshold values. The numerous soft collisions occurring between two hard events are simulated as a single, virtual event described by a multiple scattering model.

In PENELOPE, simulation geometries are constructed using quadric surfaces through the `PENGEOM` package. The materials constituting the structures defined in the geometry are generated with the code `MATERIAL` based on their density and stoichiometric composition, or by utilizing the extensive library of materials available. To control the simulation process, PENELOPE necessitates a main program. In this study, we employed the `PENMAIN` code, which is included in the PENELOPE distribution.

The simulation of electrons and positrons in PENELOPE is governed by the transport parameters: C_1, which sets the average angular deflection between two consecutive hard collisions; C_2, determining the maximum fractional energy loss permissible between two hard collisions, and W_{cc} and W_{cr}, which indicate the threshold energies for hard inelastic interactions and hard bremsstrahlung emission, respectively. Additionally, particle transport relies on absorption energies: $E_{abs}(e^-)$, $E_{abs}(e^+)$ and $E_{abs}(\gamma)$, representing the energies at which the simulation of electrons, positrons and photons, respectively, is discontinued, with the particles being absorbed in the material through which they were moving. The code also incorporates the parameter s_{max}, defining the maximum distance a particle can move in a step, and thus playing a crucial role in geometries featuring very thin structures. Users are required to assign values to these parameters for each material in the geometry. Further details can be found in the PENELOPE user manual (Salvat, 2019).

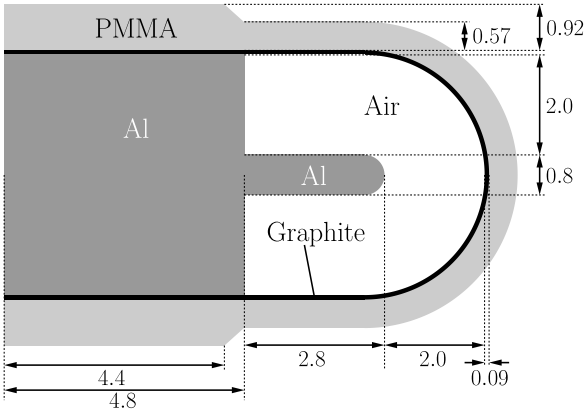

Fig. 2. Scheme of the geometry of the Semiflex 3D 31021 ionization chamber. Dimensions are in mm.

2.3. Simulations

As previously mentioned, the aim of this study is to utilize VRTs driven by the ACA to compute the beam quality correction factor for ionization chambers with a very small active volume. For this investigation, the Semiflex 3D 31021 ionization chamber (PTW, Freiburg, Germany) has been chosen as a test case because of its small sensitive volume, 0.071 cm^3. Fig. 2 provides the scheme of the geometry of this chamber that has been used in the simulations: it has been constructed based on the technical specifications provided by the company (PTW, 2017).

The Semiflex 3D 31021 is a cylindrical ionization chamber, with both the length and diameter of its sensitive volume equal to 4.8 mm. The central electrode within the chamber has a length of 2.8 mm and a diameter of 0.8 mm. The inner wall is constructed from graphite and has a thickness of 0.09 mm. The entire chamber is shielded by PMMA. Following the approach by Muir and Rogers (2010), the stem has been disregarded as its effect is deemed negligible.

The simulation setup for calculating the beam quality correction factor adhered to the TRS-398 guidelines (International Atomic Energy Agency, 2000). The absorbed dose to the active volume of the ionization chamber, denoted as $D_{c,Q}$, was determined with the ionization chamber placed inside a cubic water phantom measuring 50 cm on each side. The chamber was positioned in the axis of the radiation beam and perpendicular to it. For the ^{60}Co source, the chamber was situated at a depth of 5 cm, while for other photon beams, it was placed at a depth of 10 cm. In both cases, the source-to-surface distance was 100 cm, with a radiation field size of 10 cm × 10 cm at the phantom surface. This configuration, referred to as "setup I", aligns with the setup used in the works by Delfs et al. (2019) and Tikkanen et al. (2020).

As an application of the developed algorithm, the beam quality correction factors were also computed using a slightly different setup, which is also considered in TRS-398 guidelines (International Atomic Energy Agency, 2000). In this alternative setup, labeled as "setup II", the source-to-surface distance is 95 cm for the ^{60}Co beam and 90 cm for the other photon beams. The radiation field, with the same size as before, was defined at the chamber position.

To calculate the absorbed dose to water, $D_{w,Q}$, a cylindrical scoring voxel of water has been employed, positioned at the same location as the ionization chamber and under the same geometrical conditions. The cylindrical voxel had a radius of 1 cm and a height of 0.025 cm, consistent with the dimensions used in previous studies (Kawrakow, 2006; Wulff et al., 2008a, 2010b; Erazo and Lallena, 2013, 2016).

The reference beam has been a ^{60}Co gamma beam with its spectrum derived from the work of Mora et al. (1999). The k_{Q,Q_0} factors have been determined for various linear accelerators listed in Table 1 whose

Table 1
TPR_{10}^{20} quality indexes for the ^{60}Co beam and for the beams of different linacs used in this work and whose spectra were calculated by Sheikh-Bagheri and Rogers (2002) and Brualla et al. (2019). The values of TPR_{10}^{20} were obtained in the work by Erazo and Lallena (2013) and in the present work, using Eq. (14) and the corresponding simulated PDDs for the various beams considered. The last column shows the TPR_{10}^{20} calculated by direct application of the definition of the quality index using the ACA. The statistical uncertainties of all TPR_{10}^{20} values are below 0.01% (with a coverage factor $k = 1$).

Source		TPR_{10}^{20}	
^{60}Co[a]		0.571[d]	
Clinac LE[b]	4 MV[b]	0.644[d]	
Clinac HE[b]	6 MV[b]	0.670[d]	
	10 MV[b]	0.739[d]	
	15 MV[b]	0.763[d]	
	18 MV[b]	0.787[d]	
Siemens KD[b]	6 MV	0.679[d]	
	18 MV	0.772[d]	
Elekta SL25[b]	6 MV	0.688[d]	
	25 MV	0.799[d]	
Clinac Unique[c]	4 MV	0.634[e]	0.631[e]
Clinac C[c]	6 MV	0.652[e]	0.652[e]
	10 MV	0.727[e]	0.728[e]
	15 MV	0.751[e]	0.750[e]
	18 MV	0.771[e]	0.771[e]
	20 MV	0.774[e]	0.775[e]
TrueBeam[c]	6 MV	0.634[e]	0.634[e]
	10 MV	0.704[e]	0.703[e]

[a] Spectrum from Mora et al. (1999).
[b] Spectra from Sheikh-Bagheri and Rogers (2002).
[c] Spectra from Brualla et al. (2019).
[d] TPR_{10}^{20} calculated by Erazo and Lallena (2013).
[e] TPR_{10}^{20} calculated in the present work.

photon spectra were computed in studies by Sheikh-Bagheri and Rogers (2002) and Brualla et al. (2019). It is worth pointing out that the TrueBeam is a flattening filter free linac.

Consistent with prior studies (Wulff et al., 2008a,b; Erazo and Lallena, 2013, 2016), the photon sources have been assumed to be point sources located in vacuum. These sources emit photons with the corresponding spectrum, generating squared $10\,\text{cm} \times 10\,\text{cm}$ radiation fields at the surface of the phantom.

The TPR_{10}^{20} values of the beams taken from Mora et al. (1999) and Sheikh-Bagheri and Rogers (2002) were calculated by Erazo and Lallena (2013) using the equation

$$TPR_{10}^{20} = 1.2661 \cdot PDD_{10}^{20} - 0.0595\,, \tag{14}$$

where PDD_{10}^{20} is the ratio of the percent depth doses at 20 and 10 cm depths for a field size of $10\,\text{cm} \times 10\,\text{cm}$ defined at the phantom surface, and with a source-to-surface distance of 100 cm. According to Followill et al. (1998), this approach introduces an uncertainty smaller than ± 0.01 in the calculated TPR_{10}^{20} values. The same procedure has been applied in the present work to calculate the TPR_{10}^{20} values of the beams taken from Brualla et al. (2019). The corresponding values are shown in Table 1.

The tracking parameters utilized in all simulations conducted in this study have been selected following the same approach as in previous works (Erazo and Lallena, 2013; Erazo et al., 2014; Erazo and Lallena, 2016; Erazo et al., 2017). Specifically, $C_1 = C_2 = 0.02$ within all bodies of the geometry, except in the water phantom and the air surrounding the geometry, where $C_1 = C_2 = 0.1$. Additionally, $W_{cc} = 0.01 \cdot E_{max}$ and $W_{cr} = 0.001 \cdot E_{max}$ have been employed, with E_{max} representing the maximum energy of the initial photons. For absorption energies, the values $E_{abs}(e^-) = E_{abs}(e^+) = W_{cc}$ and $E_{abs}(\gamma) = W_{cr}$ have been considered. Finally, s_{max} has been determined, as per the manual, as one tenth of the characteristic thickness of each material in the geometry.

The simulations have been carried out by following either $3 \cdot 10^9$ showers, in the case of the validation of ACA (see Section 3.1) or $3 \cdot 10^{10}$ showers, when the k_{Q,Q_0} factors were calculated (see Section 3.3). The estimated uncertainties were $\sim 0.5\%$ in simulations incorporating VRTs with ACA, whereas in the analog simulations, where no VRTs were applied, uncertainties around 1% were found. In both cases, a coverage factor of $k = 1$ was applied.

The application of ACA has been done by considering a cylindrical grid with a radius of 5 cm and a height of 10 cm with the chamber in its center. A total of 20 virtual cells were considered in both dimensions, the importance map having 400 "geometric" virtual cells. In addition, the energy range was divided in 5 intervals and the map was scored for each particle type. The RoI was fixed as a cube with a side of 1 cm around the chamber (or the water scoring voxel in case of D_w).

All simulations whose results are shown in this work have been carried out with a processor AMD EPYC Rome 7662 having a 2.0 GHz clock and 64 cores. To calculate D_c, the simulation of 10^9 showers required between $2.3 \cdot 10^5$ s, for the ^{60}Co beam, and $1.5 \cdot 10^5$ s, for the 20 MV beam, when ACA was considered, and between $1.3 \cdot 10^6$ s, for the ^{60}Co beam, and $1.8 \cdot 10^5$ s, for the 20 MV beam, for the analog simulations (without ACA). The CPU times required to calculate D_w reduced with respect to the previous ones around 30%–40%, in the analog simulations, and between 30% and 80%, when ACA was considered. Some of the results quoted below were obtained in simulations done in parallel, by using up to 30 cores; others were found in simulations carried out in a single core.

To summarize k_{Q,Q_0} as a function of TPR_{10}^{20}, a function previously employed in earlier works (Erazo and Lallena, 2013, 2016) has been fitted to the obtained values. The function is expressed as follows:

$$f(x) = \frac{1 - \exp\left(\dfrac{x - t}{u}\right)}{1 - \exp\left(\dfrac{x_0 - t}{u}\right)}\,. \tag{15}$$

Here t and u are the fitting parameters, and x and x_0 represent the TPR_{10}^{20} values for the beam qualities Q and Q_0, respectively. It is noteworthy that this function equals 1 for the ^{60}Co source. Additionally, it is important to highlight that the validity of this fitting function is confined to the range of TPR_{10}^{20} values utilized for selecting its parameters.

3. Results and discussion

3.1. Validation of the ant colony algorithm

The initial step has been to validate the ACA specifically for the case of interest in this study, *i. e.*, the response of very small ionization chambers. The procedure involved comparing the results obtained in simulations using the ACA with those from analog simulations where no variance reduction techniques were applied. These comparisons were carried out for the ^{60}Co source, as well as for the 6 MV and 18 MV Clinac HE photon beams.

The obtained results are presented in Table 2. It is noteworthy that the values of both D_w and D_c agree in both calculations within $\pm 1.5\sigma$, with relative differences smaller than 1.5% in absolute value. Conversely, the $f_{c,Q}$ values also demonstrate agreement within $\pm 1.7\sigma$, with relative differences also below 1.5% in absolute value.

Regarding the k_{Q,Q_0} factors, the relative differences between the results of the calculations with and without ACA are less than 1% in absolute value, and the results concur within $\pm 0.8\sigma$. These findings affirm the feasibility of employing ACA in simulations involving the response of small ionization chambers.

It is also crucial to highlight that the incorporation of variance reduction techniques through ACA induces two distinct effects. Firstly, there is a decrease in the uncertainty of the calculation, with a factor ranging between 1.15 and 1.45 for D_w and between 2.57 and 2.72 for D_c. Secondly, there is a reduction in the CPU time by a factor between 4.5 and 6.5. These reductions collectively result in a notable enhancement of the calculation efficiency, with a factor between 7 and 13 for D_w and between 32 and 44 for D_c.

Table 2
Comparison of the results obtained for the Semiflex 3D 31021 ionization chamber without (n) and with (y) the ACA and the variance reductions techniques described in Section 2.1. The doses D_w and D_c are given for the ^{60}Co reference beam and for the 6 MV and 18 MV Clinac HE photon beams. Also the ratios $f_{c,Q}$, as defined by Eq. (6), and the beam quality factors k_{Q,Q_0}, given in Eq. (7), are shown. For the dose calculations, the corresponding efficiencies, as defined in Eq. (8), are also indicated. The number of showers simulated in these calculations are $3 \cdot 10^9$. Uncertainties are given with a coverage factor $k = 1$.

	ACA	^{60}Co	6 MV	18 MV
D_w (eV/g)	n	289.03 ± 0.76	370.46 ± 0.94	785.97 ± 1.51
	y	290.19 ± 0.65	371.29 ± 0.69	787.96 ± 1.04
ϵ (s^{-1})	n	0.0517	0.0949	0.1190
	y	0.3801	1.1594	1.5894
D_c (eV/g)	n	265.76 ± 2.04	348.10 ± 3.18	751.34 ± 4.27
	y	265.58 ± 0.75	343.60 ± 1.22	749.91 ± 1.66
ϵ (s^{-1})	n	0.0042	0.0053	0.0099
	y	0.1868	0.2018	0.3126
$f_{c,Q}$	n	1.0876 ± 0.0086	1.0642 ± 0.0101	1.0461 ± 0.0066
	y	1.0927 ± 0.0026	1.0806 ± 0.0020	1.0507 ± 0.0015
k_{Q,Q_0}	n		0.9785 ± 0.0122	0.9619 ± 0.0100
	y		0.9890 ± 0.0028	0.9616 ± 0.0028

Table 3
Parameters of the fitting function defined in Eq. (15), found for the k_{Q,Q_0} factors obtained for the Semiflex 3D 31021 ionization chamber in our Monte Carlo calculations. Uncertainties are given with a coverage factor $k = 1$.

	t	u
setup I	1.25397 ± 0.05776	0.146564 ± 0.02004
setup II	1.40323 ± 0.05828	0.208637 ± 0.02339

3.2. Calculation of the beam quality index

Using ACA+VRTs, the TPR_{10}^{20} values for the photon beam spectra provided by Brualla et al. (2019) have been calculated by directly applying the definition of this quality index. This involves determining the ratio of absorbed doses to water at depths of 20 cm and 10 cm, with a fixed distance of 100 cm between the source and the measurement point, and a field size at the measurement depth of 10 cm × 10 cm. The scoring voxel in these calculations is the cylinder also used to determine D_w.

In Table 1 (last two columns), the obtained results are compared to the TPR_{10}^{20} values calculated using Eq. (14). With the exception of the 4 MV beam of the Clinac Unique linac, the two sets of results are in agreement within the expected uncertainty, as quoted by Followill et al. (1998) and mentioned above.

3.3. Beam quality correction factors

After validating ACA, the beam quality correction factor, k_{Q,Q_0}, has been computed for the Semiflex 3D 31021 ionization chamber. This calculation utilized the photon beam spectra obtained by Sheikh-Bagheri and Rogers (2002) and Brualla et al. (2019).

We compared our results with those from two previous studies conducted by Delfs et al. (2019) and Tikkanen et al. (2020). In the study by Delfs et al. (2019), k_{Q,Q_0} factors were computed for five photon spectra corresponding to photon beams generated with potentials ranging between 4 and 24 MV. The calculations were performed using the EGSnrc user-code `egs_chamber` (Wulff et al., 2008b). Additionally, Delfs et al. conducted measurements of the beam quality correction factors for six clinical photon beams. In the work by Tikkanen et al. (2020), k_{Q,Q_0} values were determined for 20 photon spectra corresponding to photon beams generated with potentials ranging between 6 and 20 MV, which included five flattening filter-free beams. Similar to the study by Delfs et al. (2019), the simulations were carried out using the EGSnrc `egs_chamber` code. Fig. 3 depicts these comparisons.

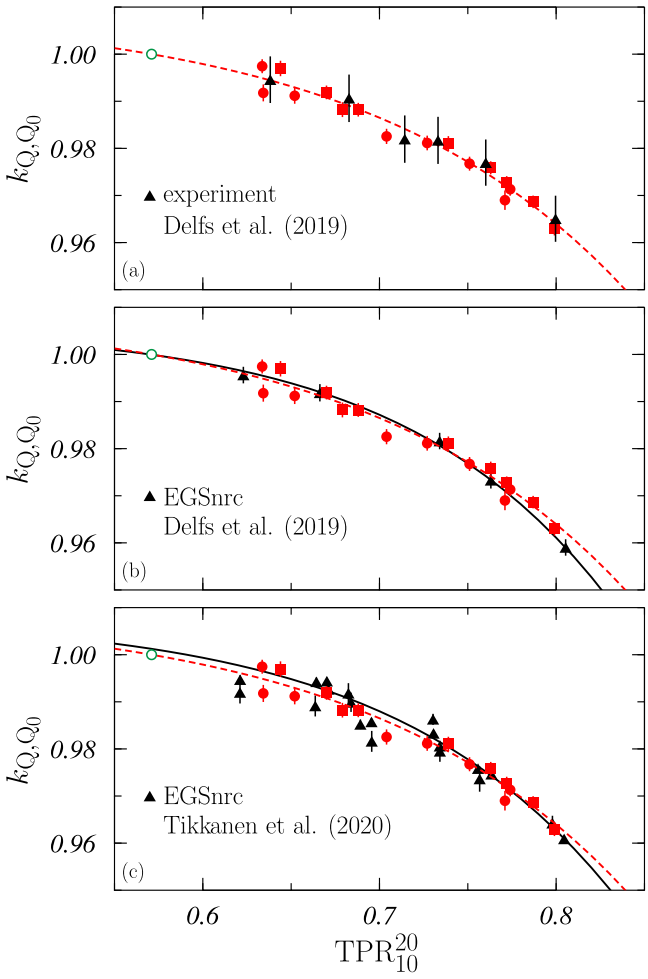

Fig. 3. Comparison of the k_{Q,Q_0} factors, as a function of TPR_{10}^{20}, obtained for the Semiflex 3D 31021 ionization chamber in our Monte Carlo simulations with ACA to those of previous studies. The results obtained for the linacs whose spectra were taken from the works by Sheikh-Bagheri and Rogers (2002) and Brualla et al. (2019) are shown by red solid squares and circles, respectively. The red dashed curve is the fit obtained for these values using the fitting function of Eq. (15). In panel (a), the black solid triangles represent the experimental data measured by Delfs et al. (2019). In panel (b), the black solid triangles are the Monte Carlo results of these authors and the black solid curve represents the fit to these values they quoted that correspond to the function $f(TPR_{10}^{20}) = 1.00585/(1.0+\exp(9.02 \cdot TPR_{10}^{20} - 10.2828))$. In panel (c), the black solid triangles show the Monte Carlo results of Tikkanen et al. (2020) and the black solid curve gives the function $f(TPR_{10}^{20}) = 1.008156/(1 + \exp(8.4027 \cdot TPR_{10}^{20} - 9.77425))$ that is the corresponding fit quoted by these authors. All uncertainties are given with a coverage factor $k = 1$. The green open circle on the left corresponds to the ^{60}Co reference beam.

The results obtained in our study, represented by red symbols, exhibit excellent agreement with the experimental values measured by Delfs et al. (2019), depicted as black solid triangles in Fig. 3a. The experimental data align closely with the red dashed curve, corresponding to the function defined in Eq. (15). This curve effectively captures our results, and its parameters are detailed in Table 3 under the setup I row.

In Fig. 3b, an overall agreement is observed between our k_{Q,Q_0} values (red symbols) and the Monte Carlo results obtained by Delfs et al. (2019), represented by black solid triangles. This agreement is reflected in the similarity between the fit presented by these authors (depicted as the black solid curve in the figure) and the fit of our results, despite differences in the fitting functions considered in both cases (refer to Eq. (15) and the figure caption for details). It is worth noting that outside the range considered in our fit, the value corresponding to

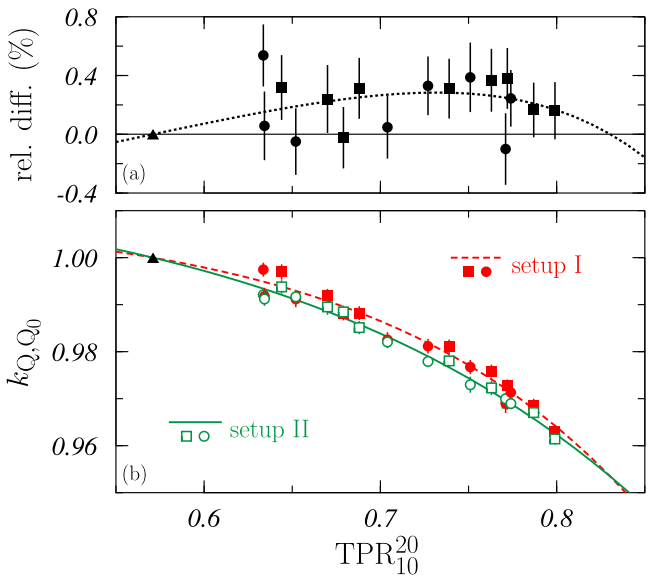

Fig. 4. Comparison of the k_{Q,Q_0} factors, as a function of TPR_{10}^{20}, obtained for the Semiflex 3D 31021 ionization chamber in our Monte Carlo simulations with the two setups considered in TRS-398 (International Atomic Energy Agency, 2000). Red solid symbols correspond to setup I, while green open symbols stand for setup II. The results obtained for the linacs whose spectra were taken from the works by Sheikh-Bagheri and Rogers (2002) are shown by squares; those corresponding to the spectra taken from Brualla et al. (2019) are plotted with circles. The red dashed and green solid curves are the fits obtained for these values using the fitting function of Eq. (15). In panel (a) the relative differences (in percentage) between both sets of results and the two fits are shown with the symbols and the dotted curve, respectively. All uncertainties are given with a coverage factor $k = 1$. The black solid triangle on the left corresponds to the ^{60}Co reference beam.

$TPR_{10}^{20} = 0.8054$ reported by Delfs et al. (2019) is slightly overestimated by our fit, the relative difference being 0.3% only.

The agreement between our results and those presented by Tikkanen et al. (2020) is also notable, as illustrated in Fig. 3c. In this case, some differences are observed between the fits to the respective data. It is important to highlight that, aside from variations in the fitting functions considered (refer to Eq. (15) and the figure caption for details), the data corresponding to the five flattening filter-free linacs (which correspond to the two data points with the smaller values of TPR_{10}^{20} and the three data points around $TPR_{10}^{20} \sim 0.7$) were excluded from the fit conducted by Tikkanen et al. Additionally, the fitting function employed by these authors does not equate to 1 for the ^{60}Co beam. As a consequence, a certain bias is evident, but the relative differences between the two fits remain below 0.6% in absolute value.

3.4. Calculation of the beam quality correction factor using setup II

As mentioned earlier, TRS-398 (International Atomic Energy Agency, 2000) proposed two different setups for determining the k_{Q,Q_0} correction factors. As a final application of ACA, corresponding calculations have been conducted with setup II (refer to Section 2.3).

Fig. 4 illustrates the comparison between the results obtained with the two setups. The majority of the k_{Q,Q_0} factors obtained with setup II (green open symbols) are slightly smaller than those corresponding to setup I (red solid symbols), with relative differences below 1% (see panel (a)). The maximum difference between the two fits (whose parameters are provided in Table 3) is 0.28%, occurring at $TPR_{10}^{20} = 0.73$. This value can be considered as a measure of the uncertainty introduced in the calculation of the k_{Q,Q_0} factors due to the experimental setup considered in the calibration of the ionization chamber.

4. Conclusions

In this study, a procedure for systematically handling various variance reduction techniques has been proposed and tested. The approach, based on an ant colony algorithm, had been successfully applied in the past to diverse problems related to radiation transport and its applications in medical physics. In this work, the algorithm has been adapted to calculate the beam quality correction factors, k_{Q,Q_0}, specifically for ionization chambers characterized by a very small active volume.

The algorithm benchmarking involved comparing doses in water and in the ionization chamber, as well as the ratios $f_{c,Q}$ and the k_{Q,Q_0} factors obtained in simulations carried out by using the algorithm and those found in analog simulations where no variance reduction techniques were applied. The findings indicate that the algorithm (i) accurately replicates the analog results within the statistical uncertainties of the simulations; (ii) yields results with uncertainties smaller than the analog ones, by a factor of up to 2.7; and (iii) demonstrates efficiency increases of up to a factor of 44.

Additionally, no significant differences have been observed in the TPR_{10}^{20} values obtained by applying the definition of this quality index compared to the commonly used approximation based on the corresponding PDD curve.

The k_{Q,Q_0} factors calculated using the algorithm for the Semiflex 3D 31021 ionization chamber exhibit good agreement with published experimental data and EGSnrc Monte Carlo calculations.

Finally, the k_{Q,Q_0} factors obtained using the two setups proposed in TRS-398 exhibit differences of less than 0.6% in absolute value, and the discrepancy between the corresponding fits is below 0.3%.

The ant colony algorithm introduced in this work for managing the application of variance reduction techniques, without the need for specific attention to the geometry setup in corresponding simulations, appears to be a highly effective tool. This is particularly advantageous for dosimetry problems involving ionization chambers with very small active volumes, which typically face challenges related to high CPU times due to their small size.

CRediT authorship contribution statement

A.M. Garví: Writing – review & editing, Writing – original draft, Visualization, Validation, Software, Methodology, Investigation, Formal analysis, Data curation, Conceptualization. **L.I. Zamora:** Writing – review & editing, Writing – original draft, Visualization, Validation, Supervision, Methodology, Investigation, Formal analysis, Data curation, Conceptualization. **M. Anguiano:** Writing – review & editing, Writing – original draft, Supervision, Resources, Project administration, Methodology, Investigation, Funding acquisition, Conceptualization. **A.M. Lallena:** Writing – review & editing, Writing – original draft, Visualization, Validation, Supervision, Software, Resources, Methodology, Investigation, Funding acquisition, Formal analysis, Data curation, Conceptualization. **S. García-Pareja:** Writing – review & editing, Writing – original draft, Visualization, Validation, Supervision, Software, Methodology, Investigation, Formal analysis, Data curation, Conceptualization.

Declaration of competing interest

The authors declare that they have no known competing financial interests or personal relationships that could have appeared to influence the work reported in this paper.

Data availability

Data will be made available on request.

Acknowledgments

This work has been partially supported by the Spanish Ministerio de Ciencia y Competitividad (PID2019-104888GB-I00, PID2022-137543NB-I00), the European Regional Development Fund (ERDF) and the Junta de Andalucía (FQM387, P18-RT-3237). Funding for open access charge by Universidad de Granada / CBUA is acknowledged.

References

Alissa, M., Zink, K., Tessier, F., Schoenfeld, A.A., Czarnecki, D., 2022. Monte Carlo calculated beam quality correction factors for two cylindrical ionization chambers in photon beams. Phys. Medica 94, 17–23.

Almond, P.R., Biggs, P.J., Coursey, B.M., Hanson, W.F., Saiful Huq, M., Nath, R., Rogers, D.W.O., 1999. AAPM's TG-51 protocol for clinical reference dosimetry of high-energy photon and electron beams. Med. Phys. 26, 1847–1870.

Bouchard, H., Seuntjens, J., Carrier, J.-F., Kawrakow, I., 2009. Ionization chamber gradient effects in nonstandard beam configurations. Med. Phys. 36, 4654–4663.

Brualla, L., Rodriguez, M., Sempau, J., Andreo, P., 2019. PENELOPE/PRIMO-calculated photon and electron spectra from clinical accelerators. Radiat. Oncol. 14 (6).

Buckley, L.A., Kawrakow, I., Rogers, D.W.O., 2004. Csnrc: correlated sampling Monte Carlo calculations using EGSnrc. Med. Phys. 31, 3425–3435.

Buckley, L.A., Rogers, D.W.O., 2006. Wall correction factors, P_{wall}, for thimble ionization chambers. Med. Phys. 33, 455–464.

Campos, L.T., Magalhães, L.A., de Almeida, C.E.V., An efficiency studying of an ion chamber simulation using variance reduction techniques with EGSnrc. J. Biomed. Phys. Eng. 9, 259–266.

Capote, R., Sánchez-Doblado, F., Leal, A., Lagares, J.I., Arráns, R., Hartmann, G.H., 2004. An EGSnrc Monte Carlo study of the microionization chamber for reference dosimetry of narrow irregular IMRT beamlets. Med. Phys. 31, 2416–2422.

Carvajal, M.A., García-Pareja, S., Guirado, D., Vilches, M., Anguiano, M., Palma, A.J., Lallena, A.M., 2009. Monte Carlo simulation using the PENELOPE code with an ant colony algorithm to study MOSFET detectors. Phys. Med. Biol. 54, 6263–6276.

Cenizo, E., García-Pareja, S., Galán, P., Bodineau, C., Caudepón, F., Casado, F.J., 2011. A jaw calibration method to provide a homogeneous dose distribution in the matching region when using a monoisocentric beam split technique. Med. Phys. 38, 2374–2381.

Delfs, B., Kapsch, R.P., Chofor, N., Looe, H.K., Harder, D., Poppe, B., 2019. A new reference-type ionization chamber with direction-independent response for use in small-field photon-beam dosimetry – An experimental and Monte Carlo study. Z. Med. Phys. 29, 39–48.

Díaz-Londoño, G., García-Pareja, S., Salvat, F., Lallena, A.M., 2015. Monte Carlo calculation of specific absorbed fractions: variance reduction techniques. Phys. Med. Biol. 60, 2625–2644.

Dorigo, M., Maniezzo, V., Colorni, A., 1996. Ant system: optimization by a colony of cooperating agents. IEEE Trans. Syst. Man Cybern. B 26, 29–41.

Erazo, F., Brualla, L., Lallena, A.M., 2014. Electron beam quality k_{Q,Q_0} factors for various ionization chambers: A Monte Carlo investigation with PENELOPE. Phys. Med. Biol. 59, 6673–6691.

Erazo, F., Brualla, L., Lallena, A.M., 2017. Computation of the electron beam quality k_{Q,Q_0} factors for the NE2571, NE2571A and NE2581A thimble ionization chambers using PENELOPE. Phys. Med.: Eur. J. Med. Phys. 38, 76–80.

Erazo, F., Lallena, A.M., 2013. Calculation of beam quality correction factors for various thimble ionization chambers using the Monte Carlo code PENELOPE. Phys. Med.: Eur. J. Med. Phys. 29, 163–170.

Erazo, F., Lallena, A.M., 2016. Photon beam quality correction factors for the NE2571A and NE2581A thimble ionization chambers using PENELOPE. Phys. Med.: Eur. J. Med. Phys. 32, 232–236.

Followill, D.S., Tailor, R.C., Tello, V.M., Hanson, W.F., 1998. An empirical relationship for determining photon beam quality in TG-21 from a ratio of percent depth doses. Med. Phys. 25, 1202–1205.

García-Pareja, S., 2012. Optimización Basada en Algoritmos de Colonias de Hormigas de Simulación Monte Carlo del Transporte de Radiación (Ph. D. Thesis). Universidad de Granada, http://hdl.handle.net/10481/29430.

García-Pareja, S., Galán, P., Manzano, F., Brualla, L., Lallena, A.M., 2010a. Ant colony algorithm implementation in electron and photon Monte Carlo transport: application to the commissioning of radiosurgery photon beams. Med. Phys. 37, 3782–3790.

García-Pareja, S., Lallena, A.M., Salvat, F., 2021. Variance-reduction methods for Monte Carlo simulation of radiation transport. Front. Phys. 9, 718873.

García-Pareja, S., Vilches, M., Lallena, A.M., 2007. Ant colony method to control variance reduction techniques in the Monte Carlo simulation of clinical electron linear accelerators. Nucl. Instrum. Methods Phys. Res. A 580, 510–513.

García-Pareja, S., Vilches, M., Lallena, A.M., 2010b. Ant colony method to control variance reduction techniques in the Monte Carlo simulation of clinical electron linear accelerators of use in cancer therapy. J. Comput. Appl. Math. 233, 1534–1541.

Giménez-Alventosa, V., Giménez, V., Ballester, F., Vijande, J., Andreo, P., 2020. Monte Carlo calculation of beam quality correction factors for PTW cylindrical ionization chambers in photon beams. Phys. Med. Biol. 65, 205005.

González-Castaño, D.M., Hartmann, G.H., Sánchez-Doblado, F., Gómez, F., Kapsch, R.-P., Pena, J., Capote, R., 2009. The determination of beam quality correction factors: Monte Carlo simulations and measurements. Phys. Med. Biol. 54, 4723–4741.

Grimbergen, T.W.M., van Dijk, E., de Vries, W., 1998. Correction factors for the NMi free-air ionization chamber for medium-energy x-rays calculated with the Monte Carlo method. Phys. Med. Biol. 43, 3207–3224.

International Atomic Energy Agency, 2000. Absorbed Dose Determination in External Beam Radiotherapy. IAEA Technical Reports Series 398, IAEA, Vienna.

Kawrakow, I., 2006. On the effective point of measurement in megavoltage photon beams. Med. Phys. 33, 1829–1839.

Kawrakow, I., Fippel, M., 2000. Investigation of variance reduction techniques for Monte Carlo photon dose calculation using XVMC. Phys. Med. Biol. 45, 2163–2183.

Kawrakow, I., Rogers, D.W.O., Walters, B., 2004. Large efficiency improvements in BEAMnrc using directional bremsstrahlung splitting. Med. Phys. 31, 2883–2898.

Ma, C.-M., Nahum, A.E., 1993. Calculation of absorbed dose ratios using correlated Monte Carlo sampling. Med. Phys. 20, 1189–1199.

Ma, C.-M., Nahum, A.E., 1995. Calculations of ion chamber displacement effect corrections for medium-energy X-ray dosimetry. Phys. Med. Biol. 40, 45–62.

Mainegra-Hing, E., Kawrakow, I., Rogers, D.W.O., 2003. Calculations for plane-parallel ion chambers in ^{60}Co beams using the EGSnrc Monte Carlo code. Med. Phys. 30, 179–189.

Malkov, V.N., Rogers, D.W.O., 2018. Monte Carlo study of ionization chamber magnetic field correction factors as a function of angle and beam quality. Med. Phys. 45, 908–925.

Mora, G.M., Maio, A., Rogers, D.W.O., 1999. Monte Carlo simulation of a typical ^{60}Co therapy source. Med. Phys. 26, 2494–2502.

Muir, B.R., Rogers, D.W.O., 2010. Monte Carlo calculations of k_Q, the beam quality conversion factor. Med. Phys. 37, 5939–5950.

Pimpinella, M., Silvi, L., Pinto, M., 2019. Calculation of k_Q factors for farmer-type ionization chambers following the recent recommendations on new key dosimetry data. Phys. Medica 57, 221–230.

PTW, 2017. Semiflex 3D Thimble Ionization Chamber for Relative and Absolute Dosimetry. PTW, Freiburg.

Reis, C.Q.M., Nicolucci, P., 2016. Assessment of ionization chamber correction factors in photon beams using a time saving strategy with PENELOPE code. Phys. Med. 32, 297–304.

Salvat, F., 2019. Penelope-2018: A Code System for Monte Carlo Simulation of Electron and Photon Transport. Document NEA/MBDAV/R(2019)1, OECD Nuclear Energy Agency, Boulogne-Billancourt.

Sánchez-Doblado, F., Andreo, P., Capote, R., Leal, A., Perucha, M., Arráns, R., Núñez, L., Mainegra, E., Lagares, J.I., Carrasco, E., 2003. Ionization chamber dosimetry of small photon fields: a Monte Carlo study on stopping-power ratios for radiosurgery and IMRT beams. Phys. Med. Biol. 48, 2081–2099.

Sánchez-Doblado, F., Capote, R., Roselló, J.V., Leal, A., Lagares, J.I., Arráns, R., Hartmann, G.H., 2005. Micro ionization chamber dosimetry in IMRT verification: Clinical implications of dosimetric errors in the PTV. Radiother. Oncol. 75, 342–348.

Sempau, J., Badal, A., Brualla, L., 2011. A PENELOPE-based system for the automated Monte Carlo simulation of clinacs and voxelized geometries — application to far-from-axis fields. Med. Phys. 38, 5887–5895.

Shanmugasundaram, S., Chandrasekaran, S., 2018. Optimization of variance reduction techniques used in EGSnrc Monte Carlo codes. J. Med. Phys. 43, 185–194.

Sheikh-Bagheri, D., Rogers, D.W.O., 2002. Monte Carlo calculation of nine megavoltage photon beam spectra using BEAM code. Med. Phys. 29, 391–402.

Tikkanen, J., Zink, K., Pimpinella, M., Teles, P., Borbinha, J., Ojala, J., Siiskonen, T., Gomà, C., Pinto, M., 2020. Calculated beam quality correction factors for ionization chambers in MV photon beams. Phys. Med. Biol. 65, 075003.

Ubrich, F., Wulff, J., Kranzer, R., Zink, K., 2008. Thimble ionization chambers in medium-energy x-ray beams and the role of constructive details of the central electrode: Monte Carlo simulations and measurements. Phys. Med. Biol. 53, 4893–4906.

Watson, P.G.F., Popovic, M., Seuntjens, J., 2018. Determination of absorbed dose to water from a miniature kilovoltage x-ray source using a parallel-plate ionization chamber. Phys. Med. Biol. 63, 015016.

Wulff, J., Heverhagen, J.T., Karle, H., Zink, K., 2010a. Investigation of correction factors for non-reference conditions in ion chamber photon dosimetry with Monte–Carlo simulations. Z. Med. Phys. 20, 25–33.

Wulff, J., Heverhagen, J.T., Zink, K., 2008a. Monte Carlo based perturbation and beam quality corrections factors for thimble ionization chambers in high energy photon beams. Phys. Med. Biol. 53, 2823–2836.

Wulff, J., Heverhagen, J.T., Zink, K., Kawrakow, I., 2010b. Investigation of systematic uncertainties in Monte Carlo-calculated beam quality correction factors. Phys. Med. Biol. 55, 4481–4493.

Wulff, J., Zink, K., Kawrakow, I., 2008b. Efficiency improvements for ion chamber calculations in high energy photon beams. Med. Phys. 35, 1328–1336.